## Laser Generated Magnetic Pulses: Comparison of Hot Electron Propagation in Conducting and Dielectric Material

A. S. Sandhu, A. K. Dharmadhikari, G. R. Kumar Tata Institute of Fundamental Research, 1 Homi Bhabha Road, Mumbai 400 005, India,

S. Sengupta, A. Das, and P. K. Kaw Institute for Plasma Research, Bhat, Gandhinagar, Ahmedabad 382428, India (Dated: November 21, 2018)

We report experimental evidence of electrostatic inhibition of fast electrons, generated in a highly resistive material upon irradiation with an intense ultra-short  $(10^{16}\,W/cm^2,\,100\,fmsec)$  laser pulse. The experiment involves measurement of temporal evolution of self-generated magnetic pulses using pump-probe polarimetry. A comparison is made between the temporal behaviour of magnetic pulses generated with Aluminum and Glass targets. It is found that in contrast to Aluminium, self-generated magnetic pulse decays much faster in glass. This is attributed to the absence of return shielding currents in glass, which results in build up of electrostatic field, which in turn inhibits the movement of fast electrons. Fitting of experimental measurements using a one dimensional model, yields estimate of conductivity of Aluminium and glass, and penetration depth of hot electrons in these materials.

PACS numbers: 52.38.Fz, 52.70.Ds, 52.70.Kz, 52.65.Rr

Interaction of intense ultrashort laser pulses with a solid leads to generation of large magnetic fields. Magnetic fields up to gigagauss magnitudes have been predicted in the overdense region of solid density plasmas [1, 2], which are created by explosive ionzation of a solid target by an incident laser. Fields comparable to stellar magnitudes ( $\geq 300$  MG) have already been experimentally realized in the laboratory with the use of superintense ultra-short laser pulses [3]. Recent studies have also established the ultrashort duration ( $\sim picosec.$ ) of these self-generated magnetic fields under femtosecond laser excitation [4, 5]. The temporal behaviour of the magnetic pulse contains crucial information about the dynamics of hot electron propagation inside a solid density material / plasma. This information about the penetration and transport of hot electrons [7] inside an overdense plasma and factors affecting it, is of utmost importance to the fast ignitor approach of fusion research [8, 9].

The pulsed high magnetic fields generated primarily near the critical density surface, result from a combination of currents, viz. the direct hot electron current which is due to copious generation of fast electrons at the critical layer via collisionless absorption of incident laser energy, and the return shielding current which is generated in response to the hot electron current [6]. The propagation of hot electrons inside the solid density target depends on whether the target is a dielectric or a conductor. In case of a dielectric (material with high classical resistivity), the return shielding current is weak, resulting in a large charge imbalance which in turn exerts a strong retarding field on the fast electrons, resulting in electrostatic inhibition. Electrostatic inhibition of hot electrons in dense matter has been seen in some experiments by

measuring K  $\alpha$  emission from layered targets. In initial experiments by Bond et. al. [10] inhibition of fast electrons due to resistive electric field was observed in low density gold targets. In contrast to a dielectric, in a conductor (material with extremely low classical resistivity ), the return shielding current nearly balances the hot electron current. Here the stopping of hot electrons occurs because of turbulence induced anomalous resistivity, the chaotic magnetic turbulence effects being generated by the presence of large gradients in the plasma currents [12, 13]. Experimental evidence of turbulence induced anomalous resistivity is presented in a recently published experiment by Sandhu et. al. [4], where they irradiate a solid aluminium target with a high intensity femtosecond laser. Since the mechanism of hot electron transport ( along with return shielding current ) and their eventual stopping is different (it is either electrostatically induced [10] or turbulence induced [4] ) in a dielectric and a conductor, it is expected that the temporal evolution of the magnetic fields which these currents generate will also be different. Thus the complex dynamics of the hot electron propagation inside a solid density material (or plasma) is reflected in the time evolution of the magnetic pulse.

Here we present experimental results on transport of hot electrons and their inhibition in both high and low resistivity media via measurements on temporal evolution of megagauss magnetic pulses. Recently, there has been a lot of experimental work on the transport of hot electrons [11], but to our knowledge no experimental result exists which gives a clear distinction between electrostatically induced and turbulence induced inhibition of fast electrons. In our experiment, this has become possible through the use of temporal measurement of magnetic pulses which is intimately related to the propagation of

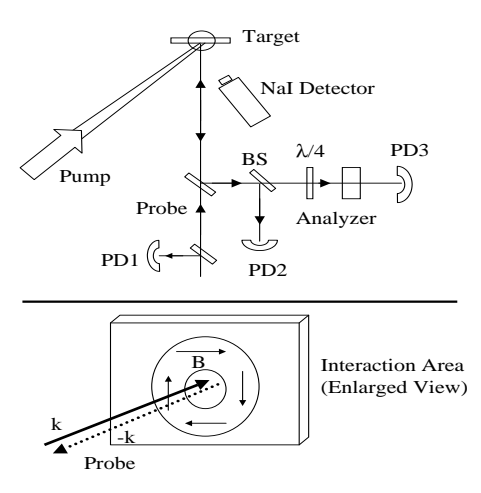


FIG. 1: Experimental setup, Target (T), Lens (L), Beam Splitter (BS), Photo Diode (PD), Half Wave Plate (HWP). Inset represents pump and probe paths in plasma. Expanded view of interaction region shows magnetic field geometry.

hot electrons inside the material. We compare two entirely different media, one conducting (solid Aluminum) and the other insulating (BK7 Glass). We use pumpprobe polarimetry to measure the ellipticity produced in a probe laser pulse due to pump-generated magnetic fields. This measured ellipticity is then analyzed numerically to deduce the magnetic field as a function of time delay between pump and probe pulses. We find that the evolution of magnetic field in aluminium and glass to be drastically different. The time required for the magnetic field to decay in glass is found to be an order of magnitude smaller than in aluminium. This is a clear indication of electrostatic inhibition of fast electrons which results from absence of return shielding currents due to very low electrical conductivity of glass. We also present an one-dimensional model (an improvement over our zero-dimensional model [4] ) for magnetic field evolution which gives an interpretation of our observations. The decay time in each case is related to the electrical conductivity ( electrostatically induced or turbulence induced), thus providing us with estimates of conductivity of glass and aluminium under conditions of elevated temperatures and pressures.

The experimental set-up is shown in figure 1. The p-polarized pump laser (100fs, 800nm) is focused at an angle of 45°, to an intensity of  $\sim 2 \times 10^{16} W cm^{-2}$  on a spot size of 20 microns. The long term contrast for the pump is  $10^5$ . The probe laser used in measurements is frequency doubled (400nm) in a thin BBO crystal, and is made  $\sim 10^3 - 10^4$  times weaker than the pump intensity and is focused at near normal incidence. In this configu-

ration, the probe penetrates beyond the critical density  $(n_c)$  for the pump laser (i.e. upto  $4n_c^{(806)}$ ), and thus samples high density region near and beyond the critical layer, where high magnetic fields are expected to exist. It should be noted that this high density region is not accessible using tangential polarimetric measurements of Faraday rotation. The input laser fluctuations are monitored with a photodiode (PD1). The reflected probe from the interaction region is split into two arms, one arm is used in PD2 to measure the reflectivity of the probe and the second arm is used in the quarter wave plate and polarizer combination (kept in front of photodiode PD3 ) to measure the polarization parameters of the probe. The reflectivity measurement serves to establish the zero delay and is used to normalize other polarimetric measurements. All the measurements are made as a function of time delay between pump and probe. Diffuse scatter is also monitored with another PD and is observed to be insignificant and constant in our temporal range of interest. In our experiment, we have used two type of targets, first one an aluminium target i.e. a conductor and second one a glass target i.e. an insulator. The BK7 glass target was coated with about half a micron thick aluminium on the front surface so that laser hitting the target generates identical hot electron temperatures in both cases. To establish that this is indeed so, we have measured the hard X-rays arising from hot electrons in the energy range from 50 to 500 keV for both the cases, under similar laser conditions with a NaI(Tl) detector. The hot electron spectra are shown in figure 2(a). The hot electron temperature obtained from the fit (shown as solid line) is observed to be approximately same ( $\sim 30 keV$ ) in both the cases (Al layer on Glass and Al metal alone). This indicates that we have identical hot electron source in both cases arising from interaction of the laser pulse with the front surface of the target. The magnetic field induced ellipticity in the probe pulse is measured using different combinations of quarter wave plate and polarizer in analyzer setup i.e. polarizer at  $0, 45, 90^{\circ}$  and  $\lambda/4$  plate at  $45^{\circ}$  and polarizer at 90° [14]. The measurement of stokes parameters in this method rules out the presence of any random depolarization. Experimental curve showing ellipticity vs time delay is also shown in figure 2(b). The significant difference is observed in time scale when we compare the two cases, that of glass and aluminum. We now numerically analyze the measured ellipticity in order to deduce the magnetic field present in the interaction region.

An electromagnetic wave travelling through a magnetized plasma with wave vector perpendicular to the quasistatic magnetic field can be analyzed in terms of two characteristic modes, the ordinary mode (O-wave) with electric field polarization vector parallel to the magnetic field and the extraordinary mode (X-wave) with electric field polarization vector perpendicular to the magnetic field [21]. These two modes have different refractive in-

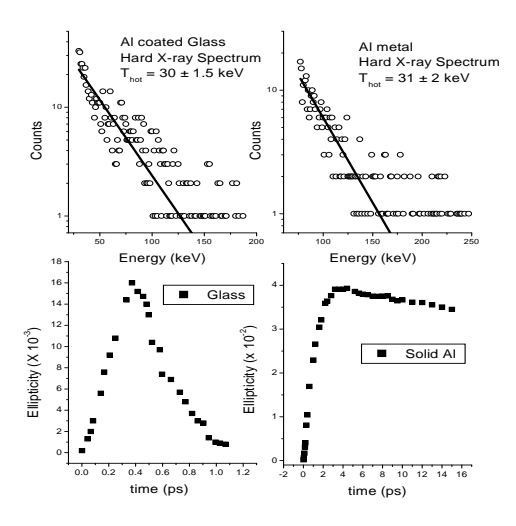


FIG. 2: The hard X-ray emmission spectra (a) for glass sample coated with 0.6 micron Al (b) pure Al metal target; in energy range 50-500 keV with laser intensity of  $2\times10^{16}~{\rm Wcm}^{-2}$ . Solid line is the exponential fit to deduce the hot electron temperature in each case. (c) Raw data for ellipticity in case of Glass coated Al (d) in case of solid Al metal.

dices, which are

$$\mu_O = \left[1 - \frac{\omega_{pe}^2}{\omega^2}\right]^{1/2} \tag{1}$$

$$\mu_X = \left[ 1 - \frac{\omega_{pe}^2(\omega^2 - \omega_{pe}^2)}{\omega^2(\omega^2 - \omega_{pe}^2 - \omega_{ce}^2)} \right]^{1/2}$$
 (2)

where  $\mu_O$  represents refractive index for O-mode and  $\mu_X$ represents refractive index for X-mode. Here  $\omega$ ,  $\omega_{pe}$ and  $\omega_{ce}$  are respectively the laser frequency, the electron plasma frequency, and the electron cyclotron frequency i.e. eB/mc. The difference in refractive indices results in accumulation of phase difference between Oand X- waves as they propagate through the plasma. This difference in phase is observed as induced ellipticity. If we represent the laser polarization in terms of stokes vector  $s = (s_1, s_2, s_3)$ ,  $s_1 = cos(2\chi)cos(2\psi)$ ,  $s_2 = cos(2\chi)sin(2\psi)$ ,  $s_3 = sin(2\chi)$ , where  $\psi$  is orientation of polarization ellipse, then the ellipticity  $\epsilon$  is given by  $\epsilon = tan(\chi)$ . The evolution of stokes vector inside the magnetized plasma is given by the difference in refractive indices of the characteristic waves i.e.  $ds/dz = \Omega(z) \times s(z)$ , where  $\Omega = (\omega/c)(\mu_O - \mu_X)$ . The solution of this polarization evolution equation is written as  $s(z) = M.s_{input}$ , where  $M_{ij}$  is the transition matrix which obeys the equation  $dM_i/dz = \Omega \times M_i$ , where  $M_i = (M_{1i}, M_{2i}, M_{3i})$  [14]. We integrate this equation numerically inside the plasma by dividing it into small slabs, where within each slab, the plasma parameters are assumed to be constant.

For the purpose of integration, the required plasma density profile is modelled by assuming that the plasma expands into vacuum at ion sound speed in a self similar fashion [17, 20], which yields an exponential density profile of the form  $n_e = n_s exp(-z/c_s t)$ , where  $n_s$ is the solid density and  $c_s = \sqrt{(ZkT_e/m_i)}$  is the ion sound speed. We have chosen the background electron temperature  $T_e = 100 eV$  [18] and the average ionization state Z = 5 [22]. At the vacuum end, which is chosen at a distance  $L_s$  from the critical layer, we put a cut off on the density ' $n_{end}$ ' which is chosen sufficiently low so that it makes practically no difference to the results. The plasma slab to be integrated over is given by  $L_s = c_s t [ln(n_{critical}/n_{end})]$ . It is found that the results are not sensitive to the chosen density profile; even the use of linear density profile yields results within acceptable error bars. In addition to the density profile, we have assumed uniform magnetic field inside the plasma column. Although, this assumption is not strictly correct, it makes little difference to the results, and is a reasonable one as shown later. The solution  $M_{ij}(z)$ , and  $s(z) = M.s_{input}$  can now be determined for any small plasma slab ( where the density is assumed to be constant ) for a given value of magnetic field B in definition of  $\Omega$ . Thus recursively solving in small steps and maintaining unitarity of M one can find the full transition matrix for whole plasma column, for any chosen density profile. From the transition matrix, the final stokes vector can be computed which in turn gives the ellipticity of the reflected probe.

In addition to the phase difference introduced by differences in refractive indices, there is an extra phase difference which aries due to slightly different turning points for O and X-wave. The X-mode has a turning point i.e. right cut-off in the dispersion diagram, earlier than the O-mode, which reflects at usual critical density. This extra path travelled by O-mode as compared to X-mode leads to an additional phase difference, which we have included in our calculation of net ellipticity. Thus the effect of magnetic field manifests itself in the form of ellipticity of the reflected probe light by both of the above mentioned processes i.e. difference in refractive indices and difference in turning points.

Using the above described procedure, for each time delay, we iteratively calculate the magnetic field B required to yield the experimentally observed ellipticity. The final plots of magnetic field for solid aluminium target and BK7 glass coated with aluminium layer are shown in fig. 3(a) and fig. 3(b) respectively. The squares represent experimental points and the solid curves, which show a reasonable fit to the experimental data are obtained using a one-dimensional model developed below. It is observed that the peak magnetic field reached in both

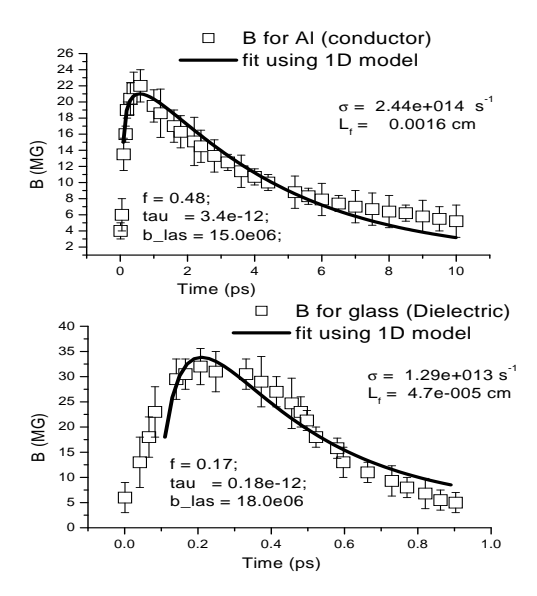


FIG. 3: Magnetic field pulse profile for (a) Glass (b) Aluminum with laser with intensity of  $2 \times 10^{16}$  Wcm<sup>-2</sup>. Solid line shows the fit for p-polarized case using a phenomenological model.

cases are of the same order ( 32MG in case of BK7 glass and 22MG in case of solid aluminium). The most striking difference between the two cases is seen in the time durations of the self-generated magnetic pulses (note different time axis of fig 4(a) and (b)). In case of BK7 glass coated with alumunium, the time duration of the magnetic pulse ( $\sim 1picosec$ ) is an order of magnitude smaller than the time duration ( $\sim 10picosec$ ) of the magnetic pulse for pure aluminium. This is a clear indication of high background resistivity of glass, which curtails the return currents and hence results in inhibition of hot electrons because of electrostatic fields. This leads to much faster resistivite decay of magnetic fields in case of glass sample as compared to solid aluminium sample, where the decay is mainly due to turbulence induced anomalous resistivity [4].

We now model the temporal evolution of magnetic field using the following equation, which describes the mechanism of quasistatic magnetic field generation under EMHD approximation.

$$\frac{\partial \vec{B}}{\partial t} = \frac{c^2}{4\pi\sigma} \nabla^2 \vec{B} + \frac{c}{\sigma} \left( \vec{\nabla} \times \vec{j}_{hot} \right) \tag{3}$$

The above equation is derived by taking the curl of the equation of motion of background plasma electrons that carry the return shielding currents,  $\vec{j}_p = (c/4\pi)(\nabla \times \vec{B}) - \vec{j}_{hot}$ , where  $\vec{j}_p = \sigma \vec{E}$ ,  $\sigma$  being the conductivity of the background plasma. The first term describes the magnetic field decay due to resistive damping of the plasma shielding currents and the second term describes the magnetic field generation due to hot electron currents. As-

suming the magnetic field to be in the azimuthal direction, equation (3) can be approximated as

$$\frac{\partial B}{\partial t} \approx -\frac{B_{\phi}}{\tau} + S(z, t) \tag{4}$$

where the diffusion term is approximated as  $B/\tau$  with  $\tau \approx (4\pi\sigma/c^2)(\Delta r)^2$ , and the source term is approximated as  $S(z,t) \approx -(c/\sigma(\Delta r))j_{hot}(z,t)$ . Here  $\Delta r$  is the laser spot radius  $\approx 10\mu$ . Our main interest lies in understanding the evolution of the magnetic field after the laser is switched off. This is because the experimental results show that, although the laser is on only for  $\sim 100fmsec.$ , the magnetic field peaks and remains on for picoseconds time duration. Taking  $B=B_{las}$  at  $t=\tau_{laser}$ , the solution of equation (4) is given by

$$B = B_{las}e^{-(t-\tau_{laser})/\tau} + e^{-t/\tau} \int_{\tau_{laser}}^{t} S(t,z,r)e^{t/\tau}dt$$

$$\approx B_{las}e^{-(t-\tau_{laser})/\tau} - e^{-t/\tau} \int_{\tau_{laser}}^{t} \frac{c}{\sigma \Delta r} j_{hot}(z,t)e^{t/\tau} dt$$

where  $j_{hot} = -en_h v_h$ ,  $n_h$  is the hot electron density and  $v_h$  is the velocity of the hot electron fluid. To make an estimate of  $n_h$  and  $v_h$ , we use the formalism given by Bell et. al. [15]. According to [15], the evolution of hot electron density  $(n_h)$  is governed by the following nonlinear diffusion equation

$$\frac{\partial n_h}{\partial t} = \frac{\partial}{\partial z} \left( \frac{\sigma T_h}{e^2 n_h} \frac{\partial n_h}{\partial z} \right) \tag{6}$$

Here  $T_h$  is the hot electron temperature. It can be shown that the above equation is valid even without the restricted assumption  $j_{total} = j_{hot} + j_p \approx 0$ , used in ref. [15]. Since our interest lies in  $t > \tau_{laser}$ , we use the solution of equation (6) in this temporal regime, as given in ref. [15]

$$n_h = \frac{2n_0 z_0}{\pi} \frac{L}{z^2 + L^2} \tag{7}$$

with

$$L(t) = z_0 \left[ \frac{5\pi\sigma T_h}{3e^2 n_0 z_0^2} (t - \tau_{laser}) + 1 \right]^{3/5}$$
 (8)

$$n_0 = \frac{2}{9} \frac{I_{abs}^2 \tau_{laser} e^2}{\sigma T_b^3} \tag{9}$$

$$z_0 = \frac{3\sigma T_h^2}{e^2 I_{abs}} \tag{10}$$

where the absorbed intensity  $I_{abs} = fI_{incident}$ , f being the fraction absorbed. Here  $n_0$  is the density of hot electrons at z = 0, at time  $t = \tau_{laser}$  and  $z_0$  is the characteristic stopping length such that  $n_0z_0$  is the total number of hot electrons produced at time  $t = \tau_{laser}$ . The

constants  $n_0$  and  $z_0$  have been derived by equating the absorbed laser energy " $I_{abs}\tau_{laser}$ " to the hot electron kinetic energy (see ref. [15]). The above solution (7) is a self-similar solution of equation (6) in which the spatial shape remains the same but it expands in time with a scale length L(t). Using the above expression for  $n_h$  and L(t), we estimate  $j_{hot}$  as

$$j_{hot} = -en_h v_h$$

$$= -e \frac{2n_0 z_0}{\pi} \frac{L}{z^2 + L^2} \left[ \alpha \frac{dL}{dt} \right]$$
 (11)

where  $v_h$ , the hot electron velocity is taken to be proportional to  $\frac{dL}{dt}$ ,  $\alpha$  being the proportionality constant. Substituting the expression for  $\frac{dL}{dt}$  in  $j_{hot}$  and using it in equation (5) along with  $\sigma \approx \frac{c^2}{4\pi(\Delta r)^2}\tau$ , we get

$$B = B_{las}e^{-y} + Ae^{-y}\tau \int_0^y \frac{(py\tau + 1)^{1/5}e^y}{z^2 + z_0^2(py\tau + 1)^{6/5}}dy \quad (12)$$

where  $y=\frac{(t-\tau_{laser})}{\tau}$ ,  $A=\frac{2cz_0\alpha T_h}{e\Delta r}$  and  $p=\frac{5\pi\sigma T_h}{3e^2n_0z_0^2}$ . We now use the above expression for B(t,z) at z=0 to model the magnetic field evolution as a function of time, for both BK7 glass coated with aluminium and solid aluminium using  $\tau$  ( which is related to conductivity  $\sigma$  ) and f ( fraction of light absorbed ) as free parameters. z=0 is the point where hot electrons are generated; so it is actually the critical density point. The proportionality contstant  $\alpha$  is taken to be unity.  $B_{las}$ , the magnetic field at time  $t=\tau_{laser}$  is 15MG and 18MG respectively for aluminium and glass. The best fit curves ( solid lines ) are shown in fig. 3(a) and fig. 3(b) respectively. From the best fit, the relevant parameters ( f and  $\tau$  ) for aluminium and glass are:

Aluminum: f = 0.5;  $\tau = 3.5$  ps Glass: f = 0.2;  $\tau = 0.2$  ps

Before presenting a discussion of our results obtained from one-dimensional modelling and numerical fit, we first justify the assumption we have made in our numerical analysis of ellipticity viz. the assumption of uniform magnetic field inside the plasma slab. Fig. 4 shows the typical magnetic field as a function of z and t obtained from our one-dimensional model. This plot is for aluminium with f and  $\tau$  as calculated above. As expected, the magnetic field diffuses in z and decreases in amplitude as time increases. Although the magnetic field Bvaries with z, we shall see below that its variation is not significant over the range of scale lengths which are relevant for our experiments. In Fig. 5, using equation (12) we have plotted the magnetic field as a function of position at a time corresponding to the peak of the magnetic field, for both aluminium and glass. In this plot, we have used the same value of f and  $\tau$  as obtained above. This plot clearly shows that the variation of magnetic field over the plasma slab is negligible. This justifies that the

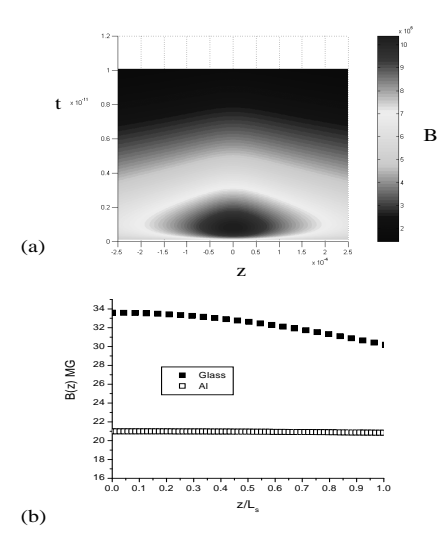


FIG. 4: (a) The z and t dependence of the magnetic field profile inside the plasma based on one dimensional model for propagation of hot electrons as disscused in the text.(b) Spatial dependence at the time corresponding to the peak magnetic field in both the cases.

assumption of uniform magnetic field in our analysis of ellipticity is a reasonable one.

We now discuss our results. From the results of the fit, it is clear that the time for magnetic field decay in aluminium is an order of magnitude larger than in glass. Calculation of conductivity using  $\sigma=(c^2/4\pi(\Delta r)^2)\tau$ , gives  $\sigma_{Al}=2.5\times 10^{14}s^{-1}$  and  $\sigma_{glass}=1.43\times 10^{13}s^{-1}$ . As of now there are no measurements of conductivity at elevated temperatures for glass and very few in aluminium. We see that resistivity of aluminium as deduced from these measurements is an order of magnitude higher than the value of resistivity deduced from reflectivity measurements by Milchberg et. al. [22]. This, we believe, is due to turbulence induced anomalous resistivity which affects the return currents. This conclusion is also supported by simulation where similar effect of anamalous resistivity and stopping of hot electrons have been seen [6]. In the case of glass, the situation is more complex as at low temperatures glass is almost non-conducting ( $\sigma \sim 0$ ). However, at elevated temperatures, as a result of target heating by collisional effects and large electric fields exceeding breakdown threshold, conductivity becomes finite. There exists observation of  $8\mu$  wide collimated ionization tracks extending upto  $150 - 300\mu$  and lasting for 60 ps in glass with a  $10^{17} Wcm^{-2}$  intensity laser [16]. Although we cannot estimate here the amount of target heating or ionization, we do get an estimate of resitivity, which we assume to be uniform in space and time. Our measurements show that neutralization of hot electron current is clearly not as effective in glass as it is in aluminium, due to high background resistivity. This results

in inhibition of hot electron propagation in glass through generation large of electrostatic fields. We now make an estimate of the penetration depth  $(L_f)$  of hot electrons using equation (8). Using the parameters  $z_0$  and  $\sigma$ from the fit and  $T_{hot}$  from observations, we get, for glass,  $L_f = 4.7 \times 10^{-5} cm \text{ in } 1 \text{ ps and } 2.1 \times 10^{-4} cm \text{ in } 10 \text{ps, and}$ for aluminium  $L_f = 1.6 \times 10^{-3} cm$  in 10ps. These numbers indicate that hot electrons are penetrating an order of magnitude more distance in a conducting background. Similar results on electrostatic inhibition have also been measured in plastic targets using  $K_{\alpha}$  emission from layered targets. This technique has its limitations due to its reliance on x-ray measurements which is a secondary diagnostic (with limitations of sensitivity, calibration, and reabsorption) and on numerical codes for interpreting Xray data.

In conclusion, the penetration of fast electrons into a target can result in very high electric field, which is not quenched by thermal return currents. This can lead to severe impediment in the flow of fast electron currents. We provide evidence of inhibition of fast electrons in an insulating media. Our results on magnetic pulse measurement and modelling in terms of hot electron currents as source, yield measurements of conductivity of conducting and dielectric media under extreme conditions. These results are very important for laser fusion schemes, which rely on ignition of hot spot by energy deposition by fast electrons.

We would like to thank D. Mathur, M. Krishnamurthy, and P. P. Rajeev for discussions and useful suggestions.

- Laser and Particle Beams 9, 841 (1991).
- [3] M. Tatarakis et al., Nature 415,280 (2002), M. Tatarakis et al., Phys. Plasmas 9, 2244 (2002).
- [4] A. S. Sandhu it et. al., Phys. Rev. Lett. 89, 225002, (2002).
- [5] M. Borghesi et al., Phys. Rev. Lett. 81, 112 (1998); Z.
   Najmudin et al., Phys. Rev. Lett. 87, 215004 (2001).
- [6] Y.Sentoku et al., Phys. Rev. E, 65, 046408 (2002), Y. Sentoku et al., Phys. Plasmas 6, 2855 (1999).
- [7] R. J. Mason and M. Tabak , Phys. Rev. Lett. 80, 524 (1998); J. R. Davies et al., Phys. Rev. E 59, 6032(1999).
- [8] E. Kolka et al., Phys. Lett. A 180, 132(1993).
- [9] M. Tabak et al., Phys. Plasmas 1, 1626 (1994).
- [10] D.J. Bond et al., Phys. Rev. Lett. 45, 252(1980) and D.J. Bond et al., Plasma Phys. 24, 91(1982).
- [11] F. Pisani et al., Phys. Rev. E 62, R5927 (2000), K. Wharton et al., Phys. Rev. Lett. 81, 822 (1998) and L. Gremillet et al., Phys. Rev. Lett. 83, 5015 (1999).
- [12] J. F. Drake et al., Phys. Rev. Lett. 73, 1251 (1994); A. Das, and P.H. Diamond, Phys. Plasmas 7, 170 (2000).
- [13] Y. Sentoku, K. Mima, P. Kaw, and K. Nishikawa, Phys. Rev. Lett. 90, 155001 (2003).
- [14] E. Collet, Polarized Light (Marcel Dekker, New York, 1993), S. E. Segre, Plasma Phys. Controlled Fusion 41, R57 (1999).
- [15] A. R. Bell, Plasma Phys. Control Fusion, 39, 653 (1997),
   A. R. Bell, J. R. Davies and S. M. Guerin Phys. Rev. E
   58, 2471 (1998).
- [16] H. Teng et. al. Phys. Rev. E 67, 026408 (2003).
- [17] P. Mora, Phys. Rev. Lett. **90**, 185002 (2003), O. L. Landen and W. E. Alley, Phys. Rev. A **46**, 5089 (1992).
- [18] K. Eidmann et. al., Phys. Rev. E 62, 1202 (2000).
- [19] M. Born and E. Wolf, Principles of Optics (Cambridge University Press, Cambridge, 1999).
- [20] W. L. Kruer, The Physics of Laser Plasma Interactions (Addison-Wesley New York 1988).
- [21] V. Krishan, Astrophysical Plasmas and Fluids(Kluwer Academic, 1999), F. F. Chen, Introduction to plasma physics and controlled fusion (Plenum Press, New York, 1974).
- [22] H. M. Milchberg et al., Phys. Rev. Lett. 61, 2364 (1988),
   A. Ng et. al., Phys. Rev. Lett. 57, 1595 (1986).

R.N. Sudan, Phys. Rev. Lett. 70, 3075 (1993); S.C. Wilks et al., Phys. Rev. Lett. 69, 1383 (1992).

J.A. Stamper *et al.*, Phys. Rev. Lett. **26**, 1012 (1971); M.
 G. Haines, Can. J. Phys, **64**, 912 (1986); J.A. Stamper,